Direct calculation of electronic Raman scattering intensities in $Cs_2NaPrCl_6$

2004 J. Phys.: Condens. Matter 16 6243

(http://iopscience.iop.org/0953-8984/16/34/022)

INSTITUTE OF PHYSICS PUBLISHING JOURNAL OF PHYSICS: CONDENSED MATTER

J. Phys.: Condens. Matter **16** (2004) 6243–6255 PII: S0953-8984(04)80455-7

Direct calculation of electronic Raman scattering intensities in $Cs_2NaPrCl_6$

Dianyuan Wang[1], **Shangda Xia**[2,3], **Michèle D Faucher**[4] **and Peter A Tanner**[3]

[1] Department of Electronics and Engineering, Jiujiang University, Jiujiang, 332005, People's Republic of China
[2] Department of Physics, University of Science and Technology of China, Hefei, Anhui 230026, People's Republic of China
[3] Department of Biology and Chemistry, City University of Hong Kong, Tat Chee Avenue, Kowloon, Hong Kong SAR, People's Republic of China
[4] 88 Avenue Jean Jaurès, 92140 Clamart, France

Received 6 May 2004
Published 13 August 2004
Online at stacks.iop.org/JPhysCM/16/6243
doi:10.1088/0953-8984/16/34/022

Abstract

The resonantly enhanced 266 nm excited electronic Raman spectrum has been recorded for polycrystalline $Cs_2NaPrCl_6$ at 10 K. Significant differences are observed in comparison with the 514.5 nm spectrum. These are rationalized by intensity calculations which, for the intermediate virtual excited (4f5d) states, utilize (I) the direct product of $4f^1$ core and $5d^1$ electronic states; (II) 4f5d coupled states obtained by using the Reid f^2 and fd programs; (III) or for the initial and final ($4f^2$) states, using the configuration-mixed wavefunctions (4fnp) obtained by a configuration interaction assisted crystal field calculation. In general, the calculated trends in intensities are fairly similar (except where the calculated corresponding energy levels differ appreciably), showing that not only the interaction between the 5d electron and the $(4f)^1$ core in the 4f5d configuration, but also the inclusion of the 4fnp configuration, do not provide the dominant contributions to the electronic Raman transition intensity of the Pr^{3+} ion. The calculated enhancements to the intensity under 266 nm, compared with 514.5 nm, excitation differ for different transitions within a given terminal multiplet term, and can vary by several orders of magnitude. The calculations are successful in pinpointing the strongest observed electronic Raman transitions, and provide an insight into the mechanistic pathways involving intermediate states.

1. Introduction

In addition to conventional luminescence and absorption spectroscopy, the energy levels of the lower multiplet terms of lanthanide ions are accessible in some cases via electronic Raman

scattering [1, 2]. This has proved especially useful where the energy level assignments are uncertain from the former two techniques [3]. However, it is then important that the relative intensities of the different electronic Raman transitions are known for a particular compound, so that secure assignments for the crystal field irreducible representations (irreps) can be made. Some previous attempts have been made in this direction for rare earth phosphates [4, 5], and also using the model cubic systems $Cs_2NaLnCl_6$, where the Ln^{3+} ion occupies a site of octahedral symmetry [6, 7]. The elpasolite systems are particularly attractive because the energy level schemes for Ln^{3+} are the simplest, and the presence of an inversion centre produces rigorous electronic Raman selection rules.

The theory of electronic Raman spectroscopy has been described in detail elsewhere [1, 8]. Basically, the electronic Raman scattering process involves the electric dipole (ED) allowed transition to a (virtual) intermediate state, and then the transition from this state to the terminal state. The initial and final states are $4f^N$ electron states, whereas the intermediate state is from an anti-parity electronic configuration, such as $4f^{N-1}5d$ (abbreviated to fd hereafter), or $4f^{N-1}5g$. Chua *et al* have performed some electronic Raman scattering intensity calculations for $Cs_2NaPrCl_6$ employing two different approaches [9]. First, the Judd–Ofelt–Axe (JOA) model [10–12] was employed. Judd and Ofelt [10, 11] introduced the closure approximation in the study of forced ED transitions of lanthanide ions in noncentrosymmetric crystals. The theory was subsequently extended by Axe [12] for two-photon transitions. In this method, the intermediate configuration is degenerate, and has an (adjustable) energy barycentre. The rank 1 tensor operators in the two particular virtual ED transitions involved in the scattering process can then be simplified as a rank 2 tensor operator acting between the initial and final states of the $4f^N$ configuration. The second approach was the Hoshina [13] or Xia [14] method. In this case the relevant excited states (fd) are synthetically produced by combining the electronic wavefunctions of a Ce^{3+} $5d^1$ electron with the states of the $4f^{N-1}$ core. The approximate energies of the resulting states are inferred from the (known) energy level structures of Ce^{3+} and the $4f^{N-1}$ (Ln^{3+}) system. This approach therefore gives some substance as to the nature of the intermediate states. However, it can be argued that since the core–d electrostatic interaction is ignored, the intermediate state wavefunctions and energy level scheme would be inaccurate. Moreover, the assumption of configuration degeneracy in the JOA approach may be considered as evidently an even more drastic one. Generally speaking, the results of the calculations for the relative intensities of electronic Raman transitions in $Cs_2NaPrCl_6$, employing these two methods, were fairly similar. The agreement with experimental results was reasonable, except for some cases where the results were not even qualitatively correct.

Recently, there has been a flurry of interest in the energy levels and intensities of interconfigurational transitions of lanthanide ions [15–18]. This has resulted in a more accurate understanding of the energies and wavefunctions of states from the fd configuration. In order to gain further insight into the electronic Raman spectra of $Cs_2NaPrCl_6$, we have therefore performed a direct calculation of the scattering intensities, using the available f^2 and fd electron wavefunctions (or including fp electron wavefunctions in the initial and final states) and the corresponding crystal field level energies. This direct calculation method has the distinct advantage that the roles of the relevant crystal field intermediate states can be pinpointed and evaluated. The calculation is described in detail herein, and new experimental results have been obtained in order to make a more extensive and accurate comparison with theory. To summarize, we aim to check and compare the various direct calculations which are based upon different approximations about the intermediate states of the fd configuration and a different fitting scheme for the f^2 configuration.

The experimental details are briefly reviewed in section 2, and the relevant structural and energy level data are presented in section 3. In section 4, the theoretical background is given,

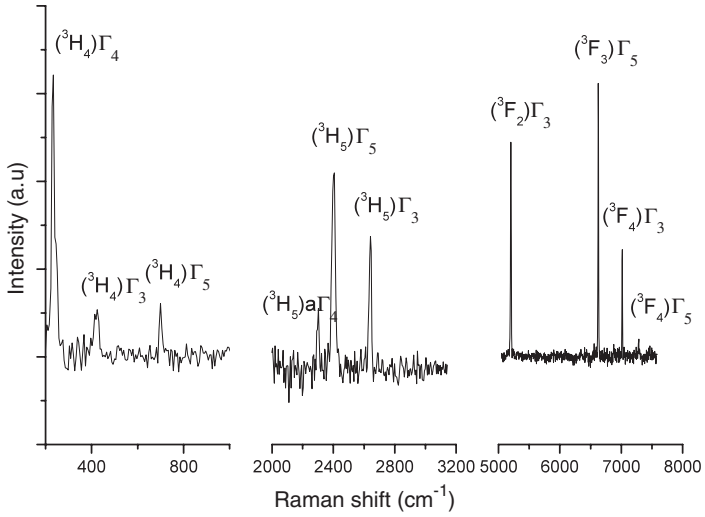

Figure 1. 266 nm excited electronic Raman spectra of $Cs_2NaPrCl_6$ at 10 K. (Separate regions are not to scale. Refer to table 4.)

and the discussion of the results is given in section 5. Finally, the major conclusions are given in section 6.

2. Experimental details

Crystals of $Cs_2NaPrCl_6$ were synthesized by the passage of dried powders from Morss method E [19] through a Bridgman furnace, in sealed quartz tubes. We have observed, using polarized Raman spectroscopy, that this preparative technique produces polycrystalline material. Resonance electronic Raman spectra were recorded at the University of Hong Kong, using the 266 nm anti-Stokes H_2-shifted line of frequency-tripled Nd-YAG laser radiation. This excitation was just below the fd states of Pr^{3+}, for which the lowest Γ_{3u} level is at 39 017 cm^{-1} in Cs_2NaYCl_6:Pr^{3+} [18]. The sample was housed in an Oxford Instruments closed cycle cryostat, with base temperature 10 K. The equipment for recording the Raman spectra has been described previously [20]. We have previously recorded the 85 and 10 K 514.5 nm excited Raman spectrum of $Cs_2NaPrCl_6$ [6]. We report the scattering intensity data from these studies, also averaged with the data from Amberger *et al* [21], in table 4.

Figure 1 shows the relevant electronic Raman features from the 266 nm (37 583 cm^{-1}) excited 10 K spectrum of $Cs_2NaPrCl_6$, and the relative intensities are also listed in table 4.

3. Energy level structure of Pr^{3+} in elpasolite crystals

The $Cs_2NaPrCl_6$ crystal undergoes a cubic to tetragonal phase transition at 152.6 K [22] or 159 K [23], but since the energy level perturbation is minor, we have assumed that the Pr^{3+} ion is located at an O_h molecular point group site at the temperature of the Raman experiment, 10 K. The $4f^2$ energy levels of Pr^{3+} in the elpasolite host lattice have been reported in [24]. The electronic ground state level is $(^3H_4)\Gamma_{1g}$, and is of rather pure parentage. The 4f5d configuration includes ten multiplets, ^3P, ^3D, ^3F, ^3G, ^3H, ^1P, ^1D, ^1F, ^1G and ^1H (140 states), belonging to 58 irreps of the O_h site symmetry group: $6\Gamma_{1u} + 5\Gamma_{2u} + 12\Gamma_{3u} + 18\Gamma_{4u} + 17\Gamma_{5u}$, whereas the

4fnp configuration includes six multiplets, ^{3}D, ^{3}F, ^{3}G, ^{1}D, ^{1}F, ^{1}G (hence 84 states), belonging to 35 irreducible representations: $3\Gamma_{1g}+4\Gamma_{2g}+7\Gamma_{3g}+10\Gamma_{4g}+11\Gamma_{5g}$. In most of the following, the subscripts g and u are omitted where they are obvious. The irreps are defined in agreement with the definitions given by Griffith for $J = 0$–6 [27].

4. Theoretical background

4.1. Transition intensity calculation

In this section, we present the methodology of the direct calculation of the electronic Raman scattering of Pr^{3+} in the elpasolite crystal lattice. This involves explicit evaluation of the transition matrix elements connecting the ground $4f^2$ (or $4f^2/4fnp$) configuration and all the fd intermediate states contributing to the electronic Raman scattering intensities.

The amplitude of the transition of the electronic Raman scattering between initial state $|\Gamma_i\gamma_i\rangle$ and final state $|\Gamma_f\gamma_f\rangle$, where the index γ labels the degeneracy of the state Γ, is written as

$$\langle\Gamma_f\gamma_f|\alpha_{\rho'\sigma'}|\Gamma_i\gamma_i\rangle, \tag{1}$$

where $\alpha_{\rho'\sigma'}$ is the Cartesian tensor, which can be expressed as

$$\alpha_{\rho'\sigma'} = -\sum_{\chi}\left\{\frac{D_{\rho'}|\Gamma_\chi\gamma_\chi\rangle\langle\Gamma_\chi\gamma_\chi|D_{\sigma'}}{\hbar\omega_\chi - \hbar\omega} + \frac{D_{\sigma'}|\Gamma_\chi\gamma_\chi\rangle\langle\Gamma_\chi\gamma_\chi|D_{\rho'}}{\hbar\omega_\chi + \hbar\omega_s}\right\}. \tag{2}$$

Both the initial and final states belong to the $4f^N$ configuration. The energy of the intermediate state $|\Gamma_\chi\gamma_\chi\rangle$, assumed to be a state of the fd configuration, is $\hbar\omega_\chi$. The polarization of the incident photon $\hbar\omega$ and scattered photon $\hbar\omega_s$ are σ' and ρ', respectively. In Cartesian coordinates, σ' and $\rho' = X, Y, Z$, where X, Y, Z are defined by the crystallographic axes of the crystal. D is the electric dipole operator.

The scattering intensities are proportional to the incoherent sums of the squares of the transition amplitudes in various polarizations:

$$\sum_{\rho',\sigma',\gamma_i,\gamma_f}|\langle\Gamma_f\gamma_f|\alpha_{\rho'\sigma'}|\Gamma_i\gamma_i\rangle|^2. \tag{3}$$

In the case of the Pr^{3+} ion in $Cs_2NaPrCl_6$, the lowest energy intermediate configuration with opposite parity is fd, and this makes the most important contribution to the electronic Raman scattering intensities.

Several different methods were employed in the calculations of the electronic Raman scattering intensities, as detailed below.

4.1.1. Calculation using 4f5d direct product wavefunctions. First, in order to investigate the importance of the Coulomb interaction between the 4f core and the 5d electron concerning the electronic Raman scattering intensity we have made a direct calculation using the direct product-type wavefunctions and corresponding energies for the 4f5d intermediate configuration, thereby ignoring this interaction. In this calculation (labelled I, hereafter) the direct product-type wavefunctions and corresponding energies for the 4f5d configuration were obtained from the direct product of the $4f^1$ (Ce^{3+}) core states and the single 5d electron (Ce^{3+}) crystal field (CF) states. The CF wavefunctions and the corresponding energies for $4f^1$ core states (and also the $4f^2$ initial and terminal states) were reproduced by using Reid's f-shell empirical programs with the input parameters reported in [2]. The CF wavefunctions for the $5d^1$ electronic states are identical to those in [28]. Moreover, the energy difference between the

lowest level of the 4f5d configuration and the ground CF level of the $4f^2$ (Pr^{3+}) configuration was taken to be 39 612 cm^{-1}. The detailed calculation method has been given in previously [9] and is not repeated herein.

4.1.2. Calculation using Reid's 4f5d coupled-type wavefunctions and energies for the intermediate states. The accurate coupled-type eigenfunctions and eigenvalues for all the states of the $4f^15d^1$ configuration are available from the f and fd programs of Reid, which take into account the electrostatic, spin–orbit and crystal field interactions, as well as other minor interactions (see, for example, [15]).

When using 4f5d coupled-type wavefunctions and energies for the intermediate states, the transition matrix element $\langle \Gamma_f \gamma_f | D^1_\rho | \Gamma_\chi \gamma_\chi \rangle$ of the rank 1 spherical tensor D^1_ρ [Note 5] can be expressed as

$$\begin{aligned}\langle 4f^2[\eta'_f S'_f L'_f J'_f]\Gamma_f\gamma_f | D^1_\rho | 4f5d[\eta_\chi S_\chi L_\chi J_\chi]\Gamma_\chi\gamma_\chi\rangle \\ = \sum_{\eta_f S_f L_f J_f M_f} \sum_{\eta S L J M} C^*_{4f^2} C_{4f5d} \langle 4f^2 \eta_f S_f L_f J_f M_f | D^1_\rho | 4f5d \eta S L J M\rangle \end{aligned} \tag{4}$$

where $C_{4f^2} = C^{[\eta'_f S'_f L'_f J'_f]\Gamma_f\gamma_f}_{4f^2,\eta_f S_f L_f J_f M_f}$ and $C_{4f5d} = C^{[\eta_\chi S_\chi L_\chi J_\chi]\Gamma_\chi\gamma_\chi}_{4f5d,\eta S L J M}$. The transition matrix element connecting the basis states of $4f^2$ and 4f5d configurations can be written as

$$\begin{aligned}&\langle 4f^2 \eta_f S_f L_f J_f M_f | D^1_\rho | 4f5d \eta S L J M\rangle \\ &\quad = \frac{2}{\sqrt{2}} \delta_{S S_f} (-1)^{2J_f + L_f - M_f + S + L} \\ &\qquad \times \sqrt{5\times 7}\sqrt{(2L+1)(2J+1)(2L_f+1)(2J_f+1)}\, e \langle 4f|r|5d\rangle \\ &\qquad \times \begin{pmatrix} 3 & 1 & 2 \\ 0 & 0 & 0 \end{pmatrix} \begin{pmatrix} J_f & 1 & J \\ -M_f & \rho & M \end{pmatrix} \begin{Bmatrix} S & L_f & J_f \\ 1 & J & L \end{Bmatrix} \begin{Bmatrix} 3 & 3 & L_f \\ 1 & L & 2 \end{Bmatrix}. \end{aligned} \tag{5}$$

The transition matrix element $\langle \Gamma_\chi \gamma_\chi | D^1_\sigma | \Gamma_i \gamma_i \rangle$ can be expressed as

$$\begin{aligned}&\langle 4f5d[\eta_\chi S_\chi L_\chi J_\chi]\Gamma_\chi\gamma_\chi | D^1_\sigma | 4f^2[\eta'_i S'_i L'_i J'_i]\Gamma_i\gamma_i\rangle \\ &\quad = \sum_{\eta S L J M} \sum_{\eta_i S_i L_i J_i M_i} C'_{4f^2} C^*_{4f5d} \langle 4f5d \eta S L J M | D^1_\sigma | 4f^2 \eta_i S_i L_i J_i M_i\rangle \\ &\quad = \sum_{\eta S L J M} \sum_{\eta_i S_i L_i J_i M_i} C'_{4f^2} C^*_{4f5d} \delta_{S S_i} (-1)^{(2J+L-M+S+L_i+1)} \\ &\qquad \times \frac{2}{\sqrt{2}} \sqrt{5\times 7}\sqrt{(2L+1)(2J+1)(2L_i+1)(2J_i+1)}\, e \langle 4f|r|5d\rangle \\ &\qquad \times \begin{pmatrix} J & 1 & J_i \\ -M & \sigma & M_i \end{pmatrix} \begin{pmatrix} 2 & 1 & 3 \\ 0 & 0 & 0 \end{pmatrix} \begin{Bmatrix} J & 1 & J_i \\ L_i & S & L \end{Bmatrix} \begin{Bmatrix} L & 1 & L_i \\ 3 & 3 & 2 \end{Bmatrix}. \end{aligned} \tag{6}$$

By replacing the terms in equation (3) with the above-mentioned equations (5) and (6), and the energies in the denominators by the fitted one for the corresponding states, the electronic Raman scattering intensity can then be calculated directly. The energy parameters employed in this calculation (hereafter labelled as calculation II) are listed in the $4f^2 + 4f5d$ column of table 1.

[5] The spherical tensor D^1_ρ is a linear combination of the cartesian tensor $D^1_{\rho'}$ as follows: $D^1_1 = -\frac{1}{\sqrt{2}}(D^1_x + iD^1_y)$, $D^1_0 = D^1_z$, $D^1_{-1} = \frac{1}{\sqrt{2}}(D^1_x - iD^1_y)$.

Table 1. Parameters used for energy level calculations for $4f^2$, $4f^2 + 4fnp$ and 4f5d configurations of Pr^{3+} in $Cs_2NaPrCl_6$.

Parameters	$4f^2$ + 4f5d (calc. II)[a]	$4f^2 + 4fnp$ + 4f5d (calc. III)[b]
F^2(f, f)	67 169	67 499
F^4(f, f)	48 106	48 274
F^6(f, f)	30 919	31 222
α	21.74	22.9
β	−629	−698
γ	1936	2035
ζ_f	745	756.1
M^0	1.76	3.33
P^2	275	0
B^4_0(f, f)	1938	3435
B^6_0(f, f)	290	606
R^2(4f, 4f, 4f, 6p)	—	−6450
R^4(4f, 4f, 4f, 6p)	—	−4333
B^4_0(f, p)	—	28 900
Δ_E(fd)	45 000	39 017
F^2(fd)	30 271[d]	18 162[c]
F^4(fd)	15 094[d]	9056[c]
G^1(fd)	12 903[d]	10 322[c]
G^3(fd)	11 160[d]	11 160[c]
G^5(fd)	8 691[d]	8691[c]
ζ_d	1 149[d]	1148[c]
B^4_0(dd)	42 357[c]	42 357[c]

[a] $4f^2$ parameters from table I in [2].
[b] Parameters from [26].
[c] From [24].
[d] 4f5d parameters from table II in [25].

4.1.3. Calculation using the energies and wavefunctions of the initial and final states obtained from a configuration interaction assisted crystal field calculation (CIACF). Since $4f^2$ crystal field states are mixed to some extent with those of other configurations of the same parity, this might induce some significant changes in the direct calculation. The calculation of electronic Raman scattering intensities requires the wavefunctions of both the ground $4f^2$ and the configurations beholding the virtual intermediate levels, just as in section 4.1.2. It was assumed as above that the latter is essentially 4f5d. This calculation is labelled III hereafter.

The wavefunctions of $4f^2$ were obtained earlier by a CIACF calculation applied to $Cs_2NaPrCl_6$ in a $|SLJM\rangle$ basis set including the ground $4f^2$ and an excited $4fnp$ configuration. The details are given in [26] where the corrective effects of the excited configuration on the calculated levels of $4f^2$ are discussed at length. Our initial guess for the excited configuration was 4f6p (a rare earth centred configuration), which has since been amended. Indeed, converging observations made on $Cs_2NaErCl_6$ and $Cs_2NaTmCl_6$ subsequently convinced us that the most efficient interacting configuration was actually a charge transfer configuration involving the p electrons of the ligands rather than the 6p electrons of the rare earth. The analysis is discussed at length in [29, 30]. The point of interest for the present investigation lies in the fact that the calculated energy levels of Pr^{3+} in $Cs_2NaPrCl_6$ are much closer to experimental values, with a mean deviation of 11.6 cm^{-1} (rather than 32.7 cm^{-1} in the standard $4f^2$ analysis). Thus, one can also expect the corresponding wavefunctions to be more accurate. Since the site symmetry at the Pr^{3+} site in the elpasolite lattice is centrosymmetric, the wavevectors of $4f^2$ contain a small admixture with the states of $4fnp$, but none with those of 4f5d.

Table 2. Energies and dominant eigenvector compositions from Reid's program for the $18\Gamma_4$ states in the 4f5d configuration of Pr^{3+}.

Γ_4 states	Energy (cm^{-1})	Dominant terms
I	41 074	68% $^1G_4$, 8% $^3H_4$, 8% $^1F_3$, 6% $^3F_4$, 4% $^3F_3$
II	42 719	43% $^3G_3$, 32% $^3F_3$, 15% $^3H_4$, 5% $^1G_4$
III	43 565	35% $^3H_5$, 27% $^3G_3$, 20% $^3F_3$, 6% $^3G_4$, 5% $^3G_5$
IV	44 415	33% $^3H_5$, 18% $^3G_4$, 16% $^3F_4$, 12% $^1G_4$
V	45 158	30% $^3F_4$, 22% $^3G_5$, 16% $^3H_6$, 10% $^3G_4$, 10% $^3H_4$
VI	45 838	32% $^3D_1$, 24% $^3G_4$, 16% $^3H_5$, 8% $^3H_4$
VII	46 705	45% $^3G_5$, 24% $^3H_6$, 7% $^3D_1$, 6% $^3H_4$, 6% $^3G_4$
VIII	47 599	46% $^3D_3$, 11% $^3H_5$, 17% $^3H_6$, 9% $^3G_5$, 6% $^3G_4$
IX	47 976	34% $^3P_1$, 30% $^3H_5$, 14% $^3G_5$, 11% $^3H_4$
X	53 055	51% $^1H_5$, 45% $^1F_3$, 2% $^1G_4$, 2% $^3H_5$
XI	57 900	48% $^1P_1$, 48% $^1H_5$, 2% $^3H_5$, 1% $^3G_5$
XII	63 968	29% $^3F_3$, 18% $^3H_5$, 17% $^3F_4$, 11% $^3G_3$, 9% $^3H_6$, 7% $^3G_5$
XIII	65 286	48% $^3D_1$, 18% $^3H_4$, 12% $^3G_4$, 9% $^3H_5$, 3% $^3F_3$, 3% $^3G_3$
XIV	65 741	42% $^3G_5$, 26% $^3F_4$, 12% $^3G_4$, 10% $^3H_6$, 3% $^3D_3$
XV	67 222	42% $^3D_3$, 31% $^3G_5$, 13% $^3H_6$, 9% $^3H_5$
XVI	68 493	59% $^3P_1$, 23% $^3H_5$, 9% $^3H_4$, 3% $^1H_5$, 2% $^3G_5$, 2% $^3G_3$
XVII	71 350	45% $^1F_3$, 44% $^1H_5$, 6% $^1G_4$, 2% $^1P_1$
XVIII	77 658	48% $^1H_5$, 47% $^1P_1$, 2% $^1F_3$, 2% $^1G_4$, 1% $^3P_1$, 1% $^3D_1$

In [24] the energy levels of 4f5d were fitted to the observed experimental levels in $Cs_2NaPrCl_6$. The electrostatic, spin–orbit and crystal field interactions were taken into account. Table 1, final column, lists the complete parameter set utilized to fit the f^2 and 4f5d levels [24, 26]. Let us recall that the introduction of the 4fnp parameters in the calculation has no impact upon the fd levels and wavefunctions. In the same way, the introduction of the 4f5d parameters has no impact on the $4f^2$ levels and wavefunctions.

In $Cs_2NaPrCl_6$, the 4f5d configuration comprises two separated sets of 84 (lower) and 56 (upper) levels, respectively reflecting the $\Gamma_{5g} + \Gamma_{3g}$ decomposition of 5d in the cubic crystal field. The total spread of the configuration amounts to 33 600 cm^{-1}, while the upper and lower sets are separated by a 8000 cm^{-1} wide gap. There exists a connection between the behaviours of $4f^2$ and 4f5d in that the features of 4f5d depend to some extent on the values the 4f crystal field parameters.

All the levels of the $4f^2$, 4fnp and 4f5d configurations were separated into ten sets corresponding to the irreducible representation components of the O_h site symmetry group: Γ_1, Γ_2, Γ_3 (2), Γ_4 (3) or Γ_5 (3). The direct calculation of electronic Raman transitions between the components of the multiplets of $4f^2$ and the ground state was then performed while the summation over intermediate states ran over the whole set of the 4f5d configuration.

5. Results and discussion

Just as for the calculation of the electric dipole absorption $4f^2 \rightarrow$ 4f5d and emission 4f5d $\rightarrow 4f^2$ intensities [24], the calculation of the electronic Raman scattering intensities is direct. Since the $4f^2$ ground state representation is $(^3H_4)\Gamma_{1g}$, and the electric dipole moment operator behaves as Γ_{4u}, only the transitions to the intermediate Γ_{4u} crystal field levels are allowed. Table 2 presents the dominant eigenvector compositions of the $18\Gamma_{4u}$ 4f5d states, as calculated using Reid's program. Note that the calculated energies reported in [24] are more accurate.

The absolute and relative intensities for 38 electronic Raman transitions of the Pr^{3+} ion in $Cs_2NaPrCl_6$ were calculated using the various kinds of wavefunctions described in section 4. In addition to the direct product state calculation (I), the results utilizing as basis sets, the 231 states of $4f^2 + 4f5d$ (II) and the 315 states of $4f^2 + 4fnp + 4f5d$ (III), are displayed in tables 3 and 4. The calculations were performed for excitation by 19 432 or 37 583 cm^{-1} radiation. The results are rounded to a few significant figures for ease of comparison. For comparison with the calculated intensities, the experimental relative intensity ratios are also listed in table 4.

First of all, the calculated intensities were all equal to zero for the transitions to $^3H_6\Gamma_2$, $^3F_3\Gamma_2$ and $^1I_6\Gamma_2$ (energy levels Nos 10, 18 and 34, respectively), in agreement with the selection rules for electronic Raman scattering in octahedral symmetry. Second, it is stressed that the electronic Raman Stokes scattering intensity is also directly proportional to $(\hbar\omega - \hbar\omega_f)^4$ [1], where $\hbar\omega_f$ is the terminal state energy. This factor is not included in the table. Thus, the electronic Raman transitions terminating upon higher $4f^2$ energy levels are relatively weaker and are not expected to be observed. Due to this factor, for example, relative to the transition from $^3H_4\Gamma_1$ to $^3H_4\Gamma_4$ at $\sim$240 cm^{-1} (level no 1), the intensities of transitions to levels 23, 27 and 29 should be decreased by factors of 0.30, 0.10 and 0.04, respectively, compared with the values listed in table 4.

In general terms, the trends are the same in calculations I, II and III. This indicates that not only the interaction between the 5d electron and the $(4f)^1$ core in the 4f5d configuration, but also the inclusion of the 4f*n*p configuration, do not provide dominant contributions to the electronic Raman transition intensity of the Pr^{3+} ion.

The *relative* intensities (normalized with respect to that for level 3) obtained utilizing either $4f^2 + 4f5d$ (II) or $4f^2 + 4fnp + 4f5d$ (III) are rather similar except in the regions where the calculated $4f^2$ levels strongly disagree with their experimental values (that is, in the calculation for $4f^2 + 4f5d$), for example, transitions 25, 26 and 35, 36. In many cases the absolute intensities (table 3) are greater for calculation III (than for I, II), since the mean energy of 4f5d is lower in calculation III. It is most notable for levels 35, 36. By contrast, the intensity for the transition to level 11 is calculated to be weaker (stronger) in calculation III than in I, II for 19 432 cm^{-1} (37 583 cm^{-1}) excitation.

Compared with that for the green laser excitation, the calculated absolute intensities for the ultraviolet laser excitation ($E_{exc} = 37\,583$ cm^{-1}) change remarkably (table 3) partly due to the $(\hbar\omega_\chi - 19\,432)^{-1} \ll (\hbar\omega_\chi - 37\,583)^{-1}$ denominator in (2). However, not only do the absolute intensities increase (usually by a factor $\sim$50), but there are also changes in the relative intensities of transitions, even within a given multiplet, since the dominant intermediate states are different for different transitions. For example, whereas transitions to the $^3H_4$ levels 2 and 3 are both enhanced by a factor of 12, the transitions to levels 1 and 4 are enhanced by factors of 66 and 101, respectively. Transitions to levels 2 and 3 thus appear weaker, with respect to the transition to level 1, under ultraviolet excitation. Thus the relative intensities of transitions can be tuned by the excitation source. Among the most enhanced transitions, that to level 4 was not observed herein or by Amberger [21] under 19 432 cm^{-1} excitation, but we clearly observe it under ultraviolet laser excitation. By contrast, although the transition to level 12 is enhanced by a factor of 883, 175 and 425 in calculations I, II and III, respectively, it is still too weak to be observed under ultraviolet excitation. The transition to level 20 is too weak to be observed under 19 432 cm^{-1} laser excitation, but since it is enhanced 1673 times (calculation III) under ultraviolet excitation, it is clearly observed at 7012 cm^{-1} (table 3). On the other hand, we do not observe the (the weakly enhanced) transition to level 15 under ultraviolet excitation, but Amberger reported a band at 5297 cm^{-1} under 514.5 nm laser excitation.

Table 3. Experimental and calculated electronic Raman transition intensities in $Cs_2NaPrCl_6$. The listed energies are experimental, calculated for f^2/fd (II) and $f^2/fp/fd$ (III), respectively [26].

			Calc. Raman scattering intensity[b]					
			$E_{exc} = 19\,432$ cm^{-1}			$E_{exc} = 37\,583$ cm^{-1}		
No	$^{2S+1}L_J\Gamma$	E (cm^{-1}) Exp.[a], f^2/fd, $f^2/fp/fd$	I[c]	II[d]	III[e]	I[c]	II[d]	III[e]
1	$^3H_4\Gamma_4$	242, 236, 247	23	16	20	3305	586	1335
2	$^3H_4\Gamma_3$	422, 406, 411	12	9	13	437	82	154
3	$^3H_4\Gamma_5$	702, 640, 721	6	5	5.3	257	47	66
4	$^3H_5a\Gamma_4$	2300, 2295, 2297	0.8	0.5	0.6	194	27	626
5	$^3H_5\Gamma_5$	2399, 2408, 2395	4.3	3.5	9	395	84	322
6	$^3H_5\Gamma_3$	2645, 2583, 2650	2.2	1.7	2.0	147	34	90
7	$^3H_5b\Gamma_4$	2763, 2689, 2750	0.01	0.008	0.009	3.2	0.5	0.38
8	$^3H_6\Gamma_3$	4386, 4402, 4373	0.00	0.00	0.09	0.003	0.3	1.2
9	$^3H_6a\Gamma_5$	4437, 4449, 4429	0.05	0.05	0.2	0.4	1.0	1.5
10	$^3H_6\Gamma_2$	4591, 4674, 4616	0.00	0.00	0.00	0.00	0.00	0.00
11	$^3H_6b\Gamma_5$	4807, 4775, 4809	0.1	0.10	0.0003	0.3	0.1	2.0
12	$^3H_6\Gamma_4$	4881, 4846, 4887	0.02	0.01	0.03	16	2.1	11
13	$^3H_6\Gamma_1$	4942, 4875, 4922	0.01	0.007	0.04	16	2.5	13
14	$^3F_2\Gamma_3$	5203, 5212, 5195	9	7	10	401	76	194
15	$^3F_2\Gamma_5$	5297, 5272, 5305	2.2	1.9	2.3	36	11	28
16	$^3F_3\Gamma_4$	6616, 6617, 6605	0.006	0.002	0.00	3	0.07	2.4
17	$^3F_3\Gamma_5$	6621, 6598, 6621	2.1	1.6	2.4	136	22	39
18	$^3F_3\Gamma_2$	6682, 6663, 6703	0.00	0.00	0.00	0.00	0.00	0.00
19	$^3F_4\Gamma_1$	6902, 6930, 6909	0.09	0.08	0.2	77	17	68
20	$^3F_4\Gamma_3$	6965, 6979, 6982	1.2	1.1	2.3	115	42	124
21	$^3F_4\Gamma_4$	7012, 6964, 6979	0.005	0.004	0.003	10	1.0	5.0
22	$^3F_4\Gamma_5$	7278, 7244, 7265	0.11	0.1	0.3	10	7.7	29
23	$^1G_4\Gamma_1$	9847, 9784, 9840	0.01	0.02	0.02	26	6.6	15
24	$^1G_4\Gamma_4$	9895, 9827, 9897	0.0003	0.02	0.003	2	2	0.07
25	$^1G_4\Gamma_3$	9910, 9845, 9921	0.006	0.001	0.02	30	2	8.4
26	$^1G_4\Gamma_5$	10 327, 10 410, 10 330	0.01	0.02	0.002	1.2	2	0.8
27	$^1D_2\Gamma_5$	16 666, 16 701, 16 671	0.60	0.25	1.5	156	8	71
28	$^1D_2\Gamma_3$	17 254, 17 198, 17 248	0.05	0.02	0.3	18	0.4	12
29	$^3P_0\Gamma_1$	20 625, 20 634, 20 612	0.4	0.2	0.09	88	1.7	4.3
30	$^1I_6\Gamma_1$	21 166, 21 083, 21 169	0.03	0.001	0.008	34	0.05	0.15
31	$^3P_1\Gamma_4$	21 218, 21 184, 21 219	0.003	0.001	0.03	32	0.3	3.4
32	$^1I_6\Gamma_4$	21 255, 21 224, 21 255	0.40	0.2	0.2	279	14	44
33	$^1I_6a\Gamma_5$	/, 21 305, 21 361	0.09	0.02	0.2	36	0.01	3.8
34	$^1I_6\Gamma_2$	21 788, 21 688, 21 779	0.00	0.00	0.00	0.00	0.00	0.00
35	$^1I_6b\Gamma_5$	21 967, 21 879, 21 976	0.008	0.01	0.4	8.7	2.2	21
36	$^1I_6\Gamma_3$	22 035, 21 935, 22 033	0.02	0.02	0.4	16	2.2	20
37	$^3P_2\Gamma_5$	22 367, 22 351, 22 376	0.8	0.4	2.3	97	4.8	45
38	$^3P_2\Gamma_3$	22 494, 22 448, 22 501	0.6	0.3	1	75	3.8	19

[a] Observed energy in the Raman spectrum, or from electronic spectra [26].
[b] Units of 10^{-11} cm^2 $e^2\langle 4f|r|5d\rangle^4/h^2c^2$. Note that the excitation line frequency dependence $(\hbar\omega - \hbar\omega_f)^4$ is not included in the table (see the text).
[c] The direct product-type 4f5d wavefunctions and corresponding energies for the intermediate states were used in the calculation.
[d] The $4f^2$ and coupled-type 4f5d wavefunctions and corresponding energies for the intermediate states were used in the calculation.
[e] The $4f^2 + 4fnp$ and 4f5d wavefunctions and corresponding energies from a CIACF calculation were used in the calculation.

Table 4. Experimental and calculated electronic Raman transition relative intensities in $Cs_2NaPrCl_6$. (The state energies are given in table 3.)

		Calc. and exp. Raman intensity ratios[a]							
		$E_{exc} = 19\,432\ cm^{-1}$				$E_{exc} = 37\,583\ cm^{-1}$			
No	$^{2S+1}L_J\Gamma$	I	II	III	Exp.[b]	I	II	III	Exp.
1	$^3H_4\Gamma_4$	3.7	3.31	3.9	1.2 ± 0.2	12.9	12.5	20.3	7.0 ± 0.6
2	$^3H_4\Gamma_3$	1.9	1.9	2.4	0.31 ± 0.07	1.7	1.7	2.3	1.2 ± 0.5
3	$^3H_4\Gamma_5$	1.00	1.00	1.00	1.0	1.00	1.00	1.00	1.0
4	$^3H_5a\Gamma_4$	0.13	0.11	0.12	n.o.	0.76	0.58	0.94	0.6 ± 0.1
5	$^3H_5\Gamma_5$	0.7	0.7	1.7	0.24 ± 0.08	1.5	1.8	4.9	2.4 ± 1.2
6	$^3H_5\Gamma_3$	0.35	0.35	0.39	n.o.	0.58	0.73	1.4	1.2 ± 0.4
7	$^3H_5b\Gamma_4$	0.002	0.002	0.002	n.o.	0.01	0.01	0.006	<0.01
8	$^3H_6\Gamma_3$	0.00	0.00	0.02	n.o.	0.00001	0.006	0.02	<0.01
9	$^3H_6a\Gamma_5$	0.009	0.01	0.03	n.o.	0.002	0.02	0.02	<0.02
10	$^3H_6\Gamma_2$	0.00	0.00	0.00	n.o.	0.00	0.00	0.00	<0.001
11	$^3H_6b\Gamma_5$	0.018	0.02	0.0001	n.o.	0.001	0.003	0.03	<0.02
12	$^3H_6\Gamma_4$	0.003	0.003	0.005	n.o.	0.06	0.04	0.17	<0.01
13	$^3H_6\Gamma_1$	0.002	0.001	0.008	n.o.	0.06	0.05	0.19	<0.01
14	$^3F_2\Gamma_3$	1.5	1.5	1.9	v.w.	1.56	1.63	2.95	∼0.5
15	$^3F_2\Gamma_5$	0.36	0.40	0.43	n.o.[c]	0.14	0.23	0.43	<0.06
16	$^3F_3\Gamma_4$	0.001	0.0004	0.00	n.o.	0.01	0.001	0.04	<0.06
17	$^3F_3\Gamma_5$	0.35	0.34	0.46	w	0.53	0.46	0.60	∼0.55
18	$^3F_3\Gamma_2$	0.00	0.00	0.00	n.o.	0.00	0.00	0.00	<0.06
19	$^3F_4\Gamma_1$	0.015	0.016	0.03	n.o.	0.30	0.36	1.03	<0.06
20	$^3F_4\Gamma_3$	0.20	0.23	0.44	n.o.	0.45	0.89	1.89	<0.06
21	$^3F_4\Gamma_4$	0.001	0.001	0.001	n.o.	0.04	0.02	0.08	∼0.2
22	$^3F_4\Gamma_5$	0.02	0.02	0.06	n.o.	0.04	0.16	0.44	∼0.04
23	$^1G_4\Gamma_1$	0.002	0.004	0.003	—	0.10	0.14	0.22	—
24	$^1G_4\Gamma_4$	0.000 05	0.005	0.0006	—	0.007	0.04	0.001	—
25	$^1G_4\Gamma_3$	0.000 1	0.0002	0.003	—	0.12	0.05	0.13	—
26	$^1G_4\Gamma_5$	0.002	0.005	0.0004	—	0.0054	0.04	0.01	—
27	$^1D_2\Gamma_5$	0.1	0.05	0.28	—	0.61	0.17	1.1	—
28	$^1D_2\Gamma_3$	0.008	0.003	0.05	—	0.07	0.01	0.19	—
29	$^3P_0\Gamma_1$	0.07	0.04	0.02	—	0.34	0.04	0.07	—
30	$^1I_6\Gamma_1$	0.004	0.0002	0.002	—	0.13	0.001	0.002	—
31	$^3P_1\Gamma_4$	0.000 4	0.0002	0.006	—	0.13	0.006	0.05	—
32	$^1I_6\Gamma_4$	0.07	0.03	0.03	—	1.09	0.30	0.66	—
33	$^1I_6a\Gamma_5$	0.01	0.004	0.04	—	0.14	0.0002	0.06	—
34	$^1I_6\Gamma_2$	0.00	0.00	0.00	—	0.00	0.00	0.00	—
35	$^1I_6b\Gamma_5$	0.001	0.003	0.07	—	0.03	0.05	0.33	—
36	$^1I_6\Gamma_3$	0.003	0.003	0.07	—	0.06	0.05	0.30	—
37	$^3P_2\Gamma_5$	0.14	0.09	0.44	—	0.38	0.10	0.68	—
38	$^3P_2\Gamma_3$	0.10	0.06	0.19	—	0.29	0.08	0.29	—

[a] Refer to the footnotes of table 3.
[b] n.o.: not observed; w: weak; v.w.: very weak.
[c] Observed in the spectrum of [21].

The direct calculation also can provide some insight into the intensity sources of the electronic Raman transitions. For $E_{exc} = 37\,583\ cm^{-1}$ and taking as an example the transition amplitudes $\langle i|\alpha_{\rho\sigma}|f\rangle$ (with $\rho = 0, \sigma = 1$) of the strongest transition from $^3H_4\Gamma_1$ to $^3H_4\Gamma_4$, the

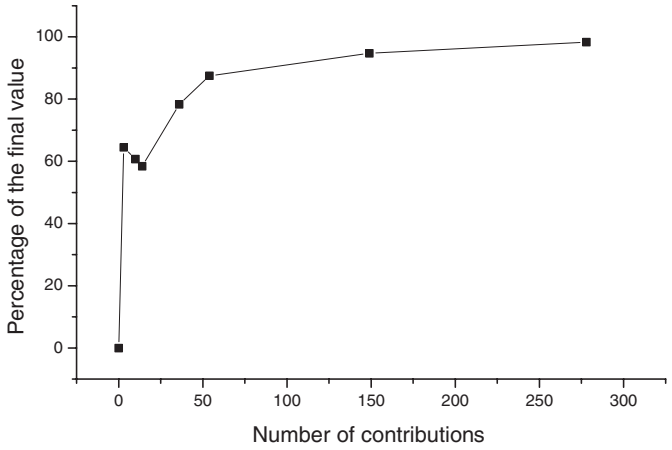

Figure 2. Convergence of the direct calculation of the transition intensity $^3H_4\Gamma_1 \rightarrow {}^3H_4\Gamma_4$ as a function of the number of contributions. Each calculation is indicated by a black square.

calculated amplitude in calculation III is equal to 47.17×10^{-6} when all the contributions are taken into account and the corresponding intensity is 222.51×10^{-11} (with units as in table 3). Since the total intensity is directly proportional to the summation of $|\langle i|\alpha_{\rho\sigma}|f\rangle|^2$ with $(\rho\sigma)$ going over (0 1), (1 0), $(-1\ 0)$, $(0\ -1)$, $(-1\ 1)$ and $(1\ -1)$, in which all the $|\langle i|\alpha_{\rho\sigma}|f\rangle|^2$ are equal, the total value given in table 3 is $6 \times 222.5 \times 10^{-11} = 1335 \times 10^{-11}$, for all of the three states of the Γ_{4g} terminal level. Table 5 details the 34 contributions larger than 0.5×10^{-6} to the amplitudes $\langle i|\alpha_{01}|f\rangle$ of this strong transition to Γ_{4g} (level 1). The total amplitude of the 34 terms is equal to 41.729×10^{-6} corresponding to an intensity of 174×10^{-11} and representing 78% of the converged value 222.51×10^{-11}. In table 5 only the matrix elements of $\alpha_{\rho\sigma}$ $(\rho = 0, \sigma = 1)$ appear, and no damping term $\alpha_{\rho\sigma}$ $(\rho = 1, \sigma = 0)$ with a large denominator is present. Notice that the contributions are signed, so cancellations may occur. Only three of the intermediate levels provide an amplitude equal to 37.897×10^{-6}, and hence contribute 64.5% of the total intensity. These efficient intermediate states lie at 40 963, 41 380 and 42 582 cm^{-1}: they are the second, third and fourth Γ_{4u} levels of the 4f5d configuration respectively. Within these intermediate states, the most active multiplets (as components of these intermediate states) are $^3G_3$, $^3H_4$, and $^3G_4$ in decreasing order. The added contributions of *all* these three multiplets account for 83% of the total intensity. Figure 2 illustrates the convergence of the calculation of the transition $^3H_4\Gamma_1 \rightarrow {}^3H_4\Gamma_4$ as a function of the number of terms considered. It is rather fast, with 83% of the total value being obtained with 54 contributions (pertaining or not to the three states quoted above).

Now, if we consider the Raman intensity associated with level 20 (Γ_3), it was mentioned above that it is strongly enhanced under UV excitation. Detailing the contributions to this intensity shows that most of it arises from interactions with the first two Γ_{4u} levels of 4f5d at 39 920 and 40 963 cm^{-1}, which explains well why it soars when the laser energy approaches 39 000 cm^{-1}.

6. Conclusions

The major conclusions from this study are:

(i) the three methods of calculation provide similar trends in electronic Raman scattering intensities for the Pr^{3+} ion in $Cs_2NaPrCl_6$;

Table 5. Contributions higher than 0.5×10^{-6} to the amplitude $\langle {}^3\mathrm{H}_4\Gamma_1 i|\alpha_{01}|{}^3\mathrm{H}_4\Gamma_4 f\rangle = -\langle {}^3\mathrm{H}_4\Gamma_4 f|\alpha_{-10}|{}^3\mathrm{H}_4\Gamma_1 i\rangle$ of the electronic Raman transition ${}^3\mathrm{H}_4\Gamma_1 \rightarrow {}^3\mathrm{H}_4\Gamma_4$. The values correspond to calculation III. (Note: the headings are: E, energy of the 4f5d state; Den., denominator; i, component of the initial level; m_1, component of the intermediate level 1; $\langle i||m_1\rangle$, matrix element of D_0 connecting $\langle i|$ and $|m_1\rangle$, i.e. $\langle i|D_0^1|m_1\rangle$; f, component of the final level; m_2, component of the intermediate level 2; $\langle m_2||f\rangle$, matrix element of D_1 connecting $\langle m_2|$ and $|f\rangle$, i.e. $\langle m_2|D_1^1|f\rangle$; Contr., contribution.)

E (cm^{-1})	Den.	i	m_1	$\langle i\|\|m_1\rangle$	m_2	f	$\langle m_2\|\|f\rangle$	Contr. $\times 10^6$
39 920	2 337	0.449 ^{3}H4 4	−0.359 ^{3}H4 4	0.363	0.046 ^{3}G3 0	−0.914 ^{3}H4-1	−0.482	−0.504
39 920	2 337	0.449 ^{3}H4-4	0.359 ^{3}H4-4	−0.363	0.046 ^{3}G3 0	−0.914 ^{3}H4-1	−0.482	−0.504
39 920	2 337	0.449 ^{3}H4 4	−0.359 ^{3}H4 4	0.363	−0.359 ^{3}H4 4	−0.345 ^{3}H4 3	−0.181	0.563
39 920	2 337	0.449 ^{3}H4-4	0.359 ^{3}H4-4	−0.363	−0.359 ^{3}H4 4	−0.345 ^{3}H4 3	−0.181	0.563
40 963	3 380	0.752 ^{3}H4 0	−0.472 ^{3}G3 0	0.610	−0.472 ^{3}G3 0	−0.914 ^{3}H4-1	−0.482	13.360
40 963	3 380	0.752 ^{3}H4 0	−0.472 ^{3}G3 0	0.610	0.137 ^{3}H4 4	−0.345 ^{3}H4 3	−0.181	−0.549
40 963	3 380	0.449 ^{3}H4 4	0.137 ^{3}H4 4	0.363	−0.472 ^{3}G3 0	−0.914 ^{3}H4-1	−0.482	−1.373
40 963	3 380	0.449 ^{3}H4-4	−0.137 ^{3}H4-4	−0.363	−0.472 ^{3}G3 0	−0.914 ^{3}H4-1	−0.482	−1.373
40 963	3 380	0.752 ^{3}H4 0	0.200 ^{3}H5 0	−0.056	−0.472 ^{3}G3 0	−0.914 ^{3}H4-1	−0.482	0.517
40 963	3 380	0.752 ^{3}H4 0	−0.472 ^{3}G3 0	0.610	−0.137 ^{1}F3 0	−0.159 ^{1}G4-1	−0.433	0.605
40 963	3 380	0.127^1 G4 0	−0.137 ^{1}F3 0	0.547	−0.472 ^{3}G3 0	−0.914 ^{3}H4-1	−0.482	0.587
40 963	3 380	0.076 ^{1}G4 4	−0.258 ^{1}G4 4	0.501	−0.472 ^{3}G3 0	−0.914 ^{3}H4-1	−0.482	0.606
40 963	3 380	0.076 ^{1}G4-4	0.258 ^{1}G4-4	−0.501	−0.472 ^{3}G 3 0	−0.914 ^{3}H4-1	−0.482	0.606
Sum 9 components at 40 963 = 13.563/14.982 (converged)								
41 380	3 797	0.752 ^{3}H4 0	−0.584 ^{3}G3 0	0.610	−0.584 ^{3}G3 0	−0.914 ^{3}H4-1	−0.482	18.194
41 380	3 797	0.752 ^{3}H4 0	−0.584 ^{3}G3 0	0.610	0.160 ^{3}H4 4	−0.345 ^{3}H4 3	−0.181	−0.710
41 380	3 797	0.752 ^{3}H4 0	−0.584 ^{3}G3 0	0.610	0.441 ^{3}H5 4	−0.345 ^{3}H4 3	−0.067	−0.721
41 380	3 797	0.449 ^{3}H4 4	−0.111 ^{3}G4 4	0.164	−0.584 ^{3}G3 0	−0.914 ^{3}H4-1	−0.482	0.554
41 380	3 797	0.449 ^{3}H4-4	0.111 ^{3}G4-4	−0.164	−0.584 ^{3}G3 0	−0.914 ^{3}H4-1	−0.482	0.554
41 380	3 797	0.449 ^{3}H4 4	0.160 ^{3}H4 4	0.363	−0.584 ^{3}G3 0	−0.914 ^{3}H4-1	−0.482	−1.775
41 380	3 797	0.449 ^{3}H4-4	−0.160 ^{3}H4-4	−0.363	−0.584 ^{3}G3 0	−0.914 ^{3}H4-1	−0.482	−1.775
41 380	3 797	0.752 ^{3}H4 0	−0.212 ^{3}H5 0	−0.056	−0.584 ^{3}G3 0	−0.914 ^{3}H4-1	−0.482	−0.604
41 380	3 797	0.752 ^{3}H4 0	−0.584 ^{3}G3 0	0.610	−0.133^{1}F3 0	−0.159 ^{1}G4-1	−0.433	0.650
41 380	3 797	0.127 ^{1}G4 0	−0.133 ^{1}F3 0	0.547	−0.584 ^{3}G3 0	−0.914 ^{3}H4-1	−0.482	0.631
Sum 10 components at 41 380 = 15.876/16.917 (converged)								
42 582	4 999	0.752 ^{3}H4 0	−0.439 ^{3}G3 0	0.610	−0.439 ^{3}G3 0	−0.914 ^{3}H4-1	−0.482	7.798
42 582	4 999	0.752 ^{3}H4 0	−0.439 ^{3}G3 0	0.610	−0.202 ^{3}H4 4	−0.345 ^{3}H4 3	−0.181	0.511
42 582	4 999	0.449 ^{3}H4 4	−0.233 ^{3}G4 4	0.164	−0.439 ^{3}G3 0	−0.914 ^{3}H4-1	−0.482	0.665
42 582	4 999	0.449 ^{3}H4-4	0.233 ^{3}G4-4	−0.164	−0.439 ^{3}G3 0	−0.914 ^{3}H4-1	−0.482	0.665
42 582	4 999	0.449 ^{3}H4 4	−0.202 ^{3}H4 4	0.363	−0.439 ^{3}G3 0	−0.914 ^{3}H4-1	−0.482	1.277
42 582	4 999	0.449 ^{3}H4-4	0.202 ^{3}H4-4	−0.363	−0.439 ^{3}G3 0	−0.914 ^{3}H4-1	−0.482	1.277
42 582	4 999	0.076 ^{1}G4 4	0.342 ^{1}G4 4	0.501	−0.439 ^{3}G3 0	−0.914 ^{3}H4-1	−0.482	−0.505
42 582	4 999	0.076 ^{1}G4-4	−0.342 ^{1}G4-4	−0.501	−0.439 ^{3}G3 0	−0.914 ^{3}H4-1	−0.482	−0.505
Sum 8 components at 42 582 = 11.183/10.953 (converged)								
44 102	6 519	0.752 ^{3}H4 0	−0.137 ^{3}G3 0	0.610	−0.137 ^{3}G3 0	−0.914 ^{3}H4-1	−0.482	0.585
45 419	7 836	0.752 ^{3}H4 0	0.166 ^{3}G3 0	0.610	0.166 ^{3}G3 0	−0.914 ^{3}H4-1	−0.482	0.712
61 960	24 377	0.752 ^{3}H4 0	−0.371 ^{3}G3 0	0.610	−0.371 ^{3}G3 0	−0.914 ^{3}H4-1	−0.482	1.146

(ii) the resonant Raman enhancements can be accounted for, and vary for individual transitions;
(iii) the detailed transition mechanisms are explicitly available from the direct calculations, and dominant pathways exist in some cases.

The intensities for levels strongly reacting with the lowest Γ_{4u} levels of the 4f5d configuration will rapidly increase when the laser wavelength approaches that energy, relatively more than levels interacting with higher (second, third, fourth) Γ_{4u} levels. One example is given here for which the experimental observation of the Raman intensity would not have been possible if the specific enhancement mentioned here had not been effective.

Acknowledgments

PAT acknowledges financial support of this work under the Hong Kong Research Grants Council Research Grant CityU 102304. SX thanks the National Natural Science Foundation of China for the support of this work under Research Grant 10274079. We are indebted to Professor M F Reid for the use of the f and fd computer programs, and also to Dr M Chua for his contribution to the early stages of this work.

References

[1] Clark R J H and Dines T J 1982 *Adv. Infrared Raman Spectrosc.* **9** 282
[2] Tanner P A, Kumar V V R K, Jayasankar C K and Reid M F 1994 *J. Alloys Compounds* **215** 349
[3] Tanner P A and Siu G G 1992 *Mol. Phys.* **75** 233
[4] Becker P C 1986 *PhD Dissertation* Lawrence Berkeley Laboratory, University of California
[5] Williams G 1988 *PhD Dissertation* Lawrence Berkeley Laboratory, University of California
[6] Tanner P A, Xia S, Liu Y-L and Ma Y 1997 *Phys. Rev.* B **55** 12182
[7] Chua M and Tanner P A 1997 *Chem. Phys.* **218** 83
[8] Nguyen A-D 1997 *Phys. Rev.* B **55** 5786
[9] Chua M, Tanner P A and Xia S 1997 *Chem. Phys. Lett.* **274** 554
[10] Judd B R 1962 *Phys. Rev.* **127** 750
[11] Ofelt G S 1962 *J. Chem. Phys.* **37** 511
[12] Axe J D 1964 *Phys. Rev.* A **136** 42
[13] Hoshina T 1980 *J. Phys. Soc. Japan* **48** 1261
[14] Xia S, Williams G M and Edelstein N M 1989 *Chem. Phys.* **138** 255
[15] Reid M F, van Pieterson L, Wegh R T and Meijerink A 2000 *Phys. Rev.* B **62** 14744
[16] Bettinelli M and Moncorgé R 2001 *J. Lumin.* **92** 287
[17] Dorenbos P 2000 *J. Lumin.* **91** 91
[18] Tanner P A, Mak C S K and Faucher M D 2001 *Chem. Phys. Lett.* **343** 309
[19] Morss L R, Siegel M, Stinger L and Edelstein N 1970 *Inorg. Chem.* **9** 1771
[20] Tanner P A, Chua M, Kwok W M and Phillips D L 1999 *Phys. Rev.* B **60** 13902
[21] Amberger H-D, Fischer R D and Rosenbauer G G 1975 *Ber. Bunsenges. Phys. Chem.* **79** 1226
[22] Aleksandrov K S, Bovina A F, Voronov V N, Gorev M V, Iskornev I V, Melnikova S V, Misjul S V, Prokert F and Flerov I N 1985 *Japan. J. Appl. Phys.* **24** 699
[23] Knudsen G P, Voss F W, Nevald R and Amberger H-D 1982 *Rare Earths in Modern Science and Technology* ed G J M^{c}Carthy, H B Silber and J J Rhyne (New York: Plenum) p 335
[24] Tanner P A, Mak C S K, Faucher M D, Kwok W M, Phillips D L and Mikhailik V 2003 *Phys. Rev.* B **67** 115102
[25] Pieterson L, Reid M F, Wegh R T, Soverna S and Meijerink A 2002 *Phys. Rev.* B **65** 045113
[26] Tanner P A, Mak C S K and Faucher M D 2001 *J. Chem. Phys.* **114** 10860
[27] Griffith J S 1980 *The Theory of Transition Metal Ions* (Cambridge: Cambridge University Press)
[28] Wang D, Ning L, Xia S and Tanner P A 2003 *J. Phys.: Condens. Matter* **15** 2681
[29] Faucher M D and Tanner P A 2003 *Mol. Phys.* **101** 983
[30] Tanner P A, Mak C S K and Faucher M D 2004 *J. Phys. Chem.* A **108** 5278